

Improving photovoltaics by adding extra terminals to extract hot carriers

Bruno Bertin-Johannet,¹ Thibaut Thuégaz,¹ Janine Splettstoesser,¹ and Robert S. Whitney²

¹*Department of Microtechnology and Nanoscience (MC2),
Chalmers University of Technology, S-412 96 Göteborg, Sweden*

²*Laboratoire de Physique et Modélisation des Milieux Condensés,
Université Grenoble Alpes and CNRS, B.P. 166, Grenoble 38042, France*

(Dated: July 18, 2025)

Photovoltaic cells usually have two terminals, one collecting electrons and the other collecting holes. Can more terminals improve such solar cells? Energy-filtering terminals could collect "hot" carriers (electrons or holes not yet relaxed to the band edge), with other terminals for low-energy carriers. For collection faster than carrier-phonon relaxation, we predict four-terminal cells with higher power output than optimal two-terminal cells—more than 40% higher for fast carrier collection. Similar effects will occur in multi-terminal thermoelectrics exploiting non-equilibrium distributions.

Introduction: Solar cells produce electrical power because solar photons create electron-hole pairs in an absorber, and the electrons are collected by one terminal (or collector), while the holes are collected by another [1, 2]. This then supplies electrical power to a load connected across the two terminals. Numerous ways to increase power outputs have been explored [3, 4]. Here we focus on a method known as *hot-carrier photovoltaics*, which was proposed 40 years ago [2, 5], but only explored in experiments more recently [6–13]. Unlike conventional photovoltaics, they are designed to get more energy from each charge carrier (electron or hole) by collecting it while it is still approximately as "hot" [14] as the thermal photon that excited it (which is at about 6000 Kelvin). More precisely, solar photons often excite electrons and holes to energies well above the semiconductor gap, and the

aim is to collect the carriers before their interaction with the substrate's phonons (at about 300 Kelvin), causes the carriers to relax to the energy of the gap. This relaxation causes the carriers to lose a significant part of their useful energy, which becomes heating of phonons which escapes unexploited into the substrate. To convert all the hot carrier's useful energy into electrical power one needs an energy-filter on the collector. This allows the cell to generate a current against a large bias by blocking the backflow of low energy carriers through the photovoltaic. However, there is a problem with this energy-filtering; it stops the collection of low energy carriers, such as those excited by low-energy solar photons, or those that have lost part of their energy to the substrate's phonons. Thus hot-carrier photovoltaics get more power per carrier collected, but they collect less carriers, making it challenging to achieve an overall higher power output.

In this Letter, we propose overcoming this problem by abandoning the conventional approach in which the absorber (where electrons and holes are excited) is coupled to only two terminals—one electron-collecting terminal and one hole-collecting terminal. We propose adding terminals to the absorber, such as four terminals in a cross-geometry (see Fig. 1). Then we can have energy-filtering terminals that collect high-energy carriers to generate larger amount of useful work per carrier, together with other terminals that collect the lower-energy carriers, so they can generate additional power (with a lower useful work per carrier). Each terminal has its own load, tuned for maximal total power output. We show that going from two to four terminals can increase the maximum power output by more than 40%.

We use a generalization of Ref. [15]'s scattering-matrix approach to multiple terminals. It accounts rates for electron-hole pair generation and recombination, carrier-carrier interactions, carrier-phonon interactions, and carrier collection by all terminals. These combine to generate the full nonthermal distribution in the absorber region discussed in End Matter.

Our approach is phenomenological, and its strength is that it is simple enough to perform the numerical opti-

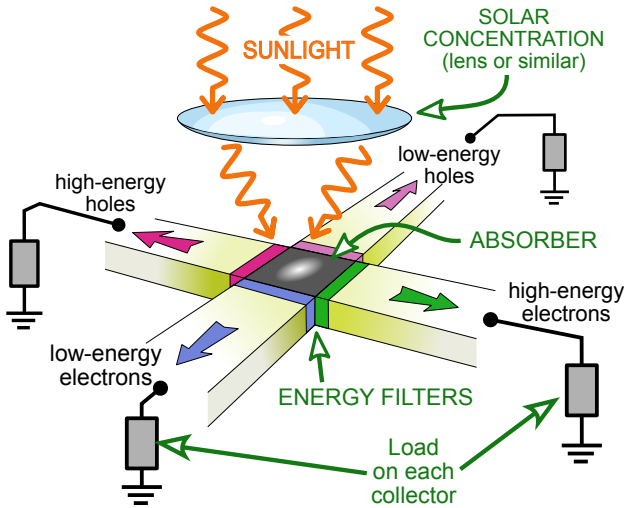


Figure 1. The four-terminal version of the multi-terminal photovoltaics proposed here. Sunlight is focused on the absorber, exciting electrons and holes. Each terminal has an energy-filter that selects the type and energy-interval of carriers that it collects from the absorber, and each terminal is coupled to its own load.

mization to maximize the power output for a very wide range of parameters. Its weakness is its simplification of electron-hole dynamics (including generation and recombination), and taking carrier-carrier and carrier-phonon interactions as energy-independent. Hence, its predictions on regimes in which adding terminals increases power should be considered as indications of regimes to be explored with the heavy numerics required for microscopic modeling (typically Green's function [16–19], density-matrix approaches [20] and ab initio techniques [21, 22]), or explored directly in experiments.

Our model predicts that adding even more terminals (each with a well-chosen energy-filter and load) allows a further increase of the power output, but the biggest increase comes when going from two to four terminals, see End Matter, which is likewise the practically most relevant case. However, we also analyze the limit of an ideal device with an infinite number of terminals, and an absorber small enough that collection is much faster than interactions. There, we show that up to 80% of the useful energy of the carriers can be turned into electrical power.

Method: We use a scattering matrix approach to model the proposed multi-terminal setup [15, 23, 24]. Multi-terminal devices have been widely considered for versatile and tunable thermoelectric effects, see e.g. Refs. [25–30], and exploiting non-thermal resources [31–36]. However, to our knowledge, there have not been studies of power outputs as one increases the number of terminals, neither for thermoelectrics nor for photovoltaics.

Here, for simplicity, we assume the electron and hole dynamics are the same (same masses, same interactions, etc), and that collectors are in symmetric pairs (for every one collecting electrons, there is an identical one for holes). Then we need only maximize the electron contribution to power output, and double it to get the full power output, but an extension to the asymmetric case is straightforward. We use a convention where $\hbar = k_B = |e| = 1$. The particle current from the absorber into electron collectors is

$$I_{\text{col},i} = \frac{1}{2\pi} \int_0^\infty d\varepsilon D_i(\varepsilon) [f_{\text{abs}}(\varepsilon) - f_{\text{col},i}(\varepsilon)], \quad (1)$$

where $D_i(\varepsilon)$ is the transmission probability for carriers at energy ε to pass between the absorber and collector terminal i . The integral starts in the middle of the absorber's band gap, $\mu_{\text{ref}} \equiv 0$, so negative energies contribute to hole currents. Terminal i has a Fermi distribution $f_{\text{col},i}(\varepsilon) = (1 + \exp[(\varepsilon - \mu_i)/T_c])^{-1}$ for room temperature ($T_c = 300$ K), its electrochemical potential, μ_i , determined by that terminal's load R_i^{load} , so $\mu_{\text{col},i} = I_{\text{col},i} R_i^{\text{load}}$. The absorber's distribution, $f_{\text{abs}}(\varepsilon)$, will be self-consistently determined by all the processes that contribute to carrier dynamics, it is usually a nonequilibrium distribution, and may be a non-monotonic function of ε .

The photovoltaic's power output in terminal i is a current I_i against a potential μ_i

$$P_{\text{col},i} = I_{\text{col},i} \mu_{\text{col},i} = I_{\text{col},i}^2 R_i^{\text{load}}. \quad (2)$$

We will tune each R_i^{load} to maximize the total power output $\sum_i P_{\text{col},i}$. In what follows, we give this power output as a ratio to the power of the incoming heat flow from the sun. For this, we assume a perfect absorber, where every solar photon creates an electron and a hole in a thermal distribution at $T_{\text{sun}} = 6000$ K, that is available to extract (see End Matter), so the incoming heat flow is

$$P_{\text{sun}}^{\text{in}} = \frac{\gamma_{\text{sun}}}{2\pi} \int_0^\infty \frac{\varepsilon d\varepsilon}{1 + \exp[\varepsilon/T_{\text{sun}}]} = 4.7 \times 10^6 \gamma_{\text{sun}}. \quad (3)$$

where γ_{sun} is a dimensionless number that is adjusted to fit the rate at which the solar collector delivers solar energy to the absorber [37]. A perfect photovoltaic would convert 95% of this heat flow into electrical power, since this is the maximum allowed by the laws of thermodynamics (Carnot efficiency is $1 - T_{\text{col}}/T_{\text{sun}}$ which is 95% for $T_{\text{sun}} = 20T_{\text{col}}$). Shockley and Queisser [1] found that a two-terminal photovoltaic's output can never exceed 44% of $P_{\text{sun}}^{\text{in}}$, and they argued that it would not exceed 30% when they added pair creation and loss mechanisms to their model [1].

Lossless limit with two-terminal. We start by recalling how a two-terminal hot-carrier photovoltaic would work in the absence of losses [38]; this is equivalent to the case of a thermoelectric, loss mechanism will be added below. When carriers absorb a solar photon, coming from a blackbody spectrum at $T_{\text{sun}} = 6000$ K, we can approximate their distribution by a Fermi distribution at T_{sun} . If all loss mechanisms are neglected, then we can treat the absorber as a gas of carriers at temperature $T_{\text{abs}} = T_{\text{sun}}$, with Fermi distribution, $f_{\text{abs}}(\varepsilon) = (1 + \exp[\varepsilon/T_{\text{sun}}])^{-1}$. The filter between absorber and collector (here, the only electron collector) is chosen to be a step-function—shown to be optimal in [29, 38, 39]—that only electrons with energies above E_0 can pass. For this, $D(\varepsilon < E_0) = 0$ and $D(\varepsilon > E_0) = 1$, and the current obeys $2\pi I_{\text{col}}/\gamma_{\text{sun}} = -T_{\text{abs}} \ln[f_{\text{abs}}(E_0)] + T_{\text{col}} \ln[f_{\text{col}}(E_0)]$. This makes the device the same as a nanoscale thermoelectric, see Ref. [30] for a review, between a hot absorber at $T_{\text{abs}} = T_{\text{sun}} = 6000$ K and a cold collector terminal at room temperature $T_{\text{col}} = 300$ K. The current and power output are shown in Fig. 2(b) for $E_0 = 10T_{\text{col}}$ and $E_0 = 30T_{\text{col}}$.

Figure 2 shows three regimes of $(\mu_{\text{col}} - E_0)/T_{\text{col}}$. The first regime is the one with a low load resistance, so $(\mu_{\text{col}} - E_0)/T_{\text{col}} \ll 0$ (dark green). Then hot carriers flow from absorber to collector, while there is negligible back-flow from collector to absorber, because no collector electron has enough energy to get over the barrier. In this regime, the current is μ_{col} -independent, but is larger for lower E_0 . Hence, the power output grows by reducing E_0 or by increasing the load resistance to raise μ_{col} . This

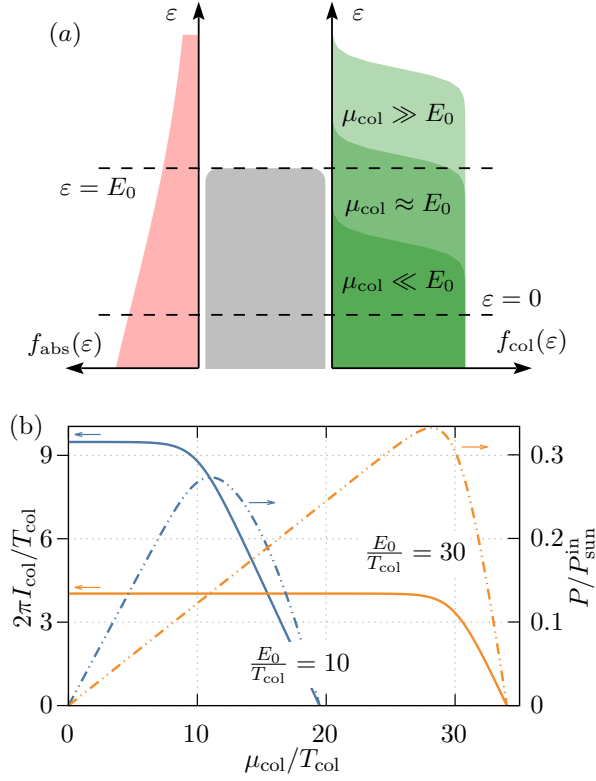


Figure 2. (a) Sketch of the energy landscape of the setup for three different chemical potentials—corresponding to three different loads—in the collector in a two-terminal setup. (b) The current (full lines) and the power (dashed lines) for two different filtering energies, $E_0/T_{\text{col}} = 10, 30$, as a function of μ_{col} , obtained from $\mu_{\text{col}} = R^{\text{load}} I_{\text{col}}$.

pushes us into a second regime where $(\mu_{\text{col}} - E_0)/T_{\text{col}} \sim 0$. There then starts to be a backflow of electrons from collector to absorber, adding a negative term to the power output that is increasingly negative as μ_{col} is increased or E_0 is reduced. Finally, the third regime is when the load resistance is large enough for $(\mu_{\text{col}} - E_0)/T_{\text{col}} \gg 0$ (light green) where the collector distribution exceeds the absorber distribution in a growing energy interval above E_0 . This gives the linear decay of I_{col} for increasingly large μ_{col} in Fig. 2(b). The decrease continues until I_{col} vanishes (infinite load resistance), then μ_{col} corresponds to the *stopping voltage* at which the generated thermocurrent is canceled by the backflow. Combining this summary of regimes of I_{col} with Eq. (2) reveals the power output (dashed lines Fig. 2) to be peaked at a finite load that corresponds to a particular value of μ_{col} . Raising the energy barrier E_0 raises the optimal μ_{col} while lowering the optimal I_{col} , so there is a clear trade-off between extracting many electrons at low energy or fewer electrons but at high energy.

Following Ref. [39] to analytically find the E_0 and μ_{col} that maximize power output, yields $f_{\text{abs}}(E_0^{\text{max}}) = f_{\text{col}}(E_0^{\text{max}})$, meaning that the filter blocks net flow,

which goes in the wrong direction and that would otherwise occur at all energies ε with $f_{\text{abs}}(\varepsilon) < f_{\text{col}}(\varepsilon)$. Then $x \ln(x) + (x+1) \ln(x+1) = 0$ [39], where $x = \exp[-\mu_{\text{col}}^{\text{max}}/(T_{\text{abs}} - T_{\text{col}})]$, yielding maximum power at $\mu_{\text{col}}^{\text{max}} = 21.7T_{\text{col}}$ and $E_0^{\text{max}} = 22.89T_{\text{col}}$. Hence,

$$P_{2\text{term}}^{\text{max}} = 0.34P_{\text{sun}}^{\text{in}}, \quad (4)$$

meaning that the maximum power output is 34% of the incoming solar heat-flow.

Lossless limit with four terminals. To circumvent the tradeoff between extracting many electrons at low energy or extracting fewer electrons at high energy, we propose the multi-terminal setup in Fig. 1 and 3(a), where low- and high-energy electrons go to different collectors. As a first step we consider the lossless case, which is equivalent to a thermoelectric, and address losses subsequently. We assume collector A is for higher-energy electrons, with a step-function filter, while collector B is for lower-energy electrons with an energy filter of boxcar-shape [40],

$$D_A(\varepsilon) = \begin{cases} 0 & \text{if } \varepsilon \leq E_0 \\ 1 & \text{if } \varepsilon > E_0, \end{cases} \quad (5a)$$

$$D_B(\varepsilon) = \begin{cases} 1 & \text{if } E_2 < \varepsilon < E_1 \\ 0 & \text{otherwise.} \end{cases} \quad (5b)$$

In Fig. 3(b) we show the total power output P_{tot} in this setup, with numerically optimized values of E_1 , E_2 , and of the two collector loads R_A^{load} , R_B^{load} for any given E_0 . The physics is similar to that outlined for two terminals, but the increased number of parameters makes it hard to predict the optimal configuration, without doing the full optimization. Other shapes of $D_{A,B}(\varepsilon)$ can be considered, and our End Matter shows that smooth functions of ε have a worse performance.

The higher-energy filter of collector A, is similar to the above two-terminal case, and shows a contribution to the generated power P_A (orange line), which has a maximum for $E_0 = 22.89T_{\text{col}}$. In contrast, the lower-energy filter on collector B has P_B (blue line) that increases with E_0 , until it is generating all the power (because E_1 is so high that no electrons enter collector A). At optimal E_0 ,

$$P_{4\text{term}}^{\text{max}} = 0.48P_{\text{sun}}^{\text{in}}, \quad (6)$$

so it converts 48% of the sun's heat energy into electrical power. This is more than 40% more power output than the ideal two-terminal photovoltaic in Eq. (4).

Lossless limit with infinitely many terminals. We now ask if adding even more terminals further increases the power output. Our End Matter's Fig. 6 shows that this is the case, but that the improvement of adding terminals becomes less the more terminals one adds. A crude fit to those results is $P(N) = P_{N \rightarrow \infty}^{\text{max}} \times (1 - \frac{1}{N+1})$ for N electron terminals (so a four-terminal device has $N = 2$), with the $N \rightarrow \infty$ limit being $P_{N \rightarrow \infty}^{\text{max}} \simeq 0.8P_{\text{sun}}^{\text{in}}$. Thus, under ideal

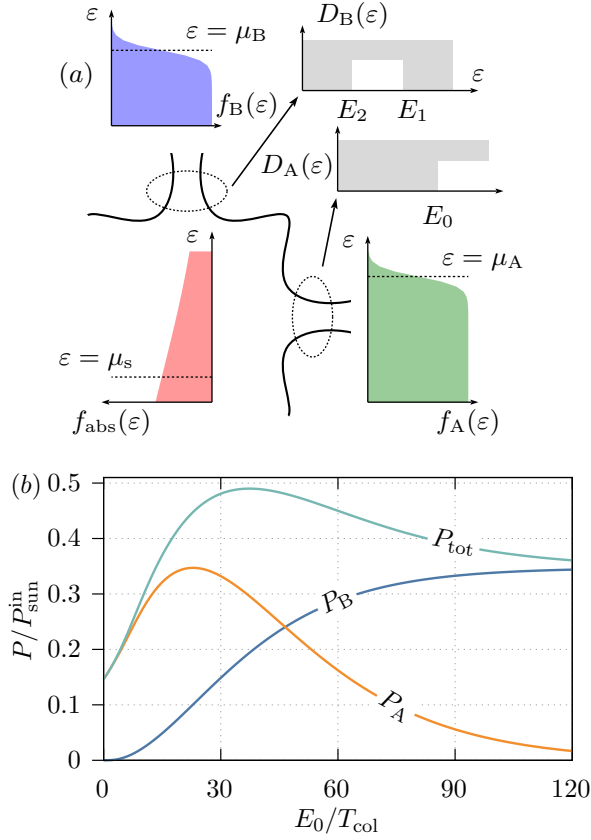


Figure 3. (a) Sketch of the electron terminals for a four-terminal setup, showing sketches of their energy-filter's transmission probabilities, Eqs. (5), as white on a gray background. (b) Total power optimized for filter boundaries E_1, E_2 and collector chemical potential μ_A, μ_B as function of E_0 . Also the separate components P_A, P_B to the optimized total power are shown.

conditions, an infinite number of terminals converts 80% of the sun's heat energy into electrical power.

Four-terminal device with losses. We now reintroduce the loss mechanisms—specifically electron-electron interactions, carrier-phonon interactions, and electron-hole recombinations—that complicate the analysis of the hot-electron photovoltaics. We also include a realistic semiconductor gap, taking InAs [41] for which $E_g = 0.68T_{sun} = 13.6T_{col}$. So there are no electronic states in the energy window from 0 to $E_g/2$.

The interactions and recombinations are modelled using a multi-terminal version of the phenomenological model in Ref. [15], that treats each such effect with a Büttiker probe [42–44]. In the End Matter we show the absorber distribution to be a weighted average of the probe distributions

$$f_{abs}(\epsilon) = \frac{\sum_i \gamma_i(\epsilon) f_i(\epsilon)}{\sum_i \gamma_i(\epsilon)}. \quad (7)$$

with i being summed over six distributions $i \in \{\text{sun},$

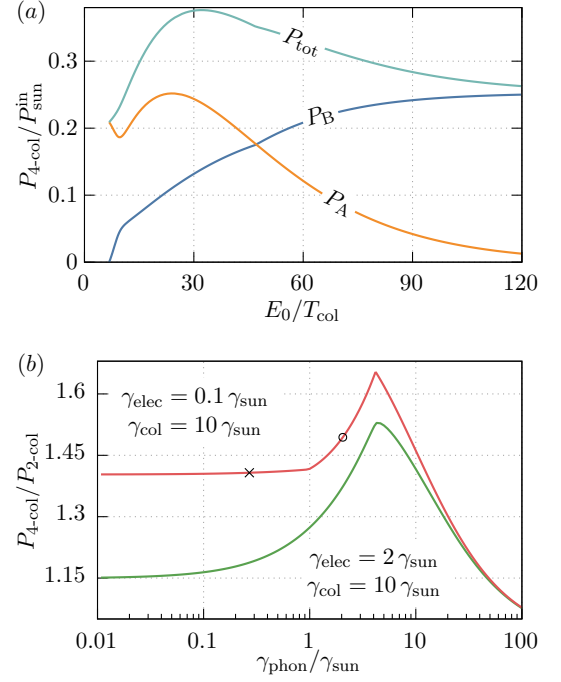


Figure 4. (a) Optimized power in a four-terminal solar cell as function of the energy E_0 between low- and high-energy filter. The coupling parameters chosen in this figure are $\gamma_{col}/\gamma_{sun} = 10$, $\gamma_{elec}/\gamma_{sun} = 0.1$, $\gamma_{phon}/\gamma_{sun} = 2$, $\gamma_{rec}/\gamma_{sun} = 0.01$. (b) Ratio between the optimized power in the four-terminal device (two collector pairs) with respect to the two-terminal case (one collector pair) as a function of the electron-phonon coupling strength. Two different cases of thermalization rates are shown. The circle corresponds to panel (a). The cross shows the parameters of Fig. 5.

phon, rec, col_A, col_B, elec}. The rates of the different interactions are given by dimensionless parameters, $\{\gamma_i\}$, with γ_{sun} giving the rate at which solar photons create electron-hole pairs. Figure 4 shows results of a numerical optimization for a plausible choice of these relative rates [9], when we maximize total power output by adjusting E_1, E_2, R_A^{load} and R_B^{load} .

In Fig. 4(b), we compare the optimal two- and four-terminal photovoltaics for these parameters, and we see that the optimized four-terminal photovoltaic outperforms the optimized two-terminal one (taking same rates of interactions and recombination for the two devices). This only ceases to be true in the limit where the rate of electron-phonon interactions becomes much larger than all other rates (meaning all "hot" carriers relax to the band-edge before they can be collected). Thus four-terminals are significantly better than two-terminals under realistic (as well as ideal) conditions.

We note that the carrier distribution in the absorber, $f_{abs}(\epsilon)$, is often non-trivial and non-monotonic (see End Matter). The collectors have a back-action on this distribution, sometimes even causing a dip in the carrier distribution at energies where carriers flow through the

filters into the collectors. This complexity implies that no simple arguments will give ideal filter parameters. Instead, we believe that a numerical optimization is the only way to maximize the power output.

Conclusion. We have shown that going from standard two-terminal to multi-terminal setups allows significantly more power output in hot-carrier solar cells. An ideal four-terminal device (in which low and high-energy carriers are filtered into different collectors with different loads) produces over 40% more power than an ideal two-terminal device. In more realistic devices, whenever loss mechanisms are slower than carrier generation and collection, similar improvements are found for four-terminals compared to two-terminals.

We expect this multi-terminal strategy to be relevant beyond photovoltaics, and could be applied to a broad range of nanoscale devices (such as thermoelectrics) that produce useful work from heat or even from the waste energy in non-equilibrium distributions.

Acknowledgments.— We thank Ludovico Tesser and Krishna Lyn Delima for helpful discussions. We were encouraged in this work by Adam Burke and Heiner Linke. Funding from the Knut and Alice Wallenberg Foundation via the Fellowship program (B.B-J.,J.S.) and from the European Research Council (ERC) under the European Union’s Horizon Europe research and innovation program (101088169/NanoRecycle) (J.S.) is gratefully acknowledged. Furthermore, R.W. acknowledges the support of the French National Research Agency (ANR) through the project “TQT” (ANR-20-CE30-0028), the project “QuRes” (ANR-PRC-CES47-0019), and the OECQ project that is financed by the French state (via France 2030) and Next Generation EU (via France Relance).

END MATTER

Non-equilibrium distribution inside the absorber

In order to model the distribution function in the absorber we model the competing effects and environments following Ref. [15]. A sketch of this model is shown in Fig. 5(a). Here, electron-hole pair creation above the bandgap by incident photons is modeled via a Fermi distribution at $\mu_{\text{sun}} = 0$ and T_{sun} which can be assumed to be of the order of the sun temperature, as previously. Energy relaxation to the phonons is modeled by a distribution at T_{phon} , typically given by room temperature, and a floating electrochemical potential μ_{phon} guaranteeing particle conservation. Furthermore, recombination of quasiparticle pairs is described by a probe at $T_{\text{rec}} = T_{\text{phon}}$ and $\mu_{\text{rec}} = 0$. The effect of the two collector pairs is described by the distributions $f_{\text{col},i}$ with an energy-dependent coupling of the filters, $\gamma_{\text{col},i}(\varepsilon) \equiv \gamma_{\text{col}} D_i(\varepsilon)$. Finally, thermalization via electron-electron interaction is modeled via a floating probe with electrochemical potential μ_{elec} and temperature T_{elec} which adjust to con-

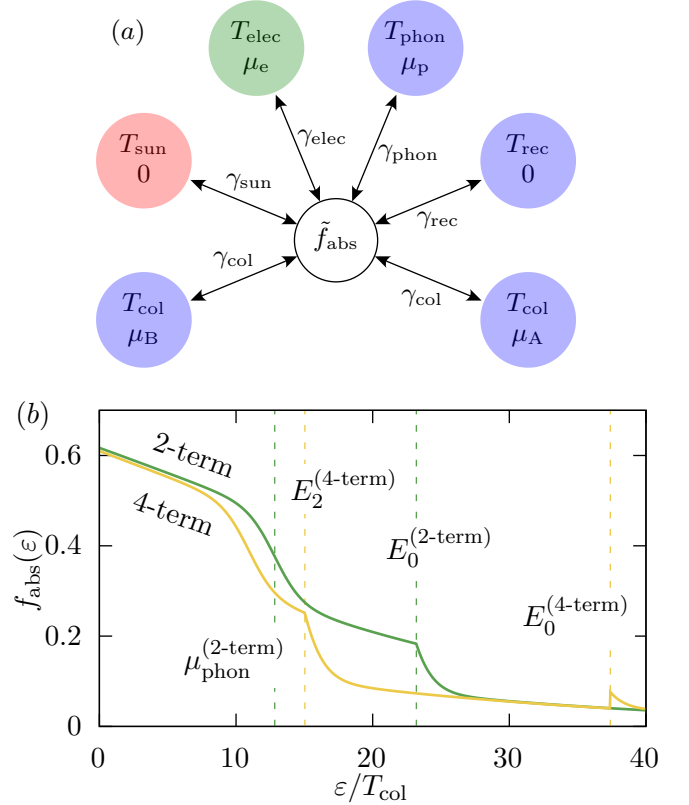


Figure 5. (a) Sketch of the multi-probe strategy to model the non-equilibrium absorber distribution [15]. (b) Electron distribution functions inside the absorber both in the case of the two-terminal and four-terminal case. The parameters correspond to $\gamma_{\text{col}} = 10\gamma_{\text{sun}}$, $\gamma_{\text{elec}} = 0.1\gamma_{\text{sun}}$, $\gamma_{\text{phon}} = 0.27\gamma_{\text{sun}}$, $\gamma_{\text{rec}} = 0.01\gamma_{\text{sun}}$.

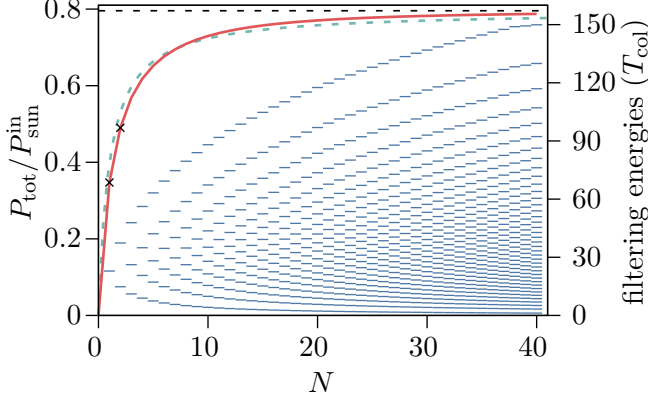


Figure 6. Total generated power output, optimized over all filter positions ($E_\alpha - \delta\varepsilon$, see Eq. (8)), indicated by fine blue lines) and corresponding loads, as function of the number of filters (red line). The two crosses correspond to the maximal power in the two- and four-terminal case. We furthermore show $P_{N \rightarrow \infty}^{\max}$, the power obtained for an infinite number of filters, see Eq. 12, dashed black line), together with a simple fit: $P(N) = P_{N \rightarrow \infty}^{\max} \times (1 - \frac{1}{N+1})$ (green dashed line).

serve particle- and energy currents. The interplay of these effects leads to an absorber distribution f_{abs} , which is typically nonthermal. Details of the modeling can be found in Refs. [15, 38].

We show two explicit example for nonequilibrium absorber distributions in Fig. 5(b), taking the parameter configuration indicated by a cross in Fig. 4. We observe steps arising in the distribution at the positions of the energy filters with close to thermal distributions in between the steps. Note that in the multi-terminal case, the distribution is not necessarily monotonic.

Increased number of filters

In the main text, we have shown that the addition of a second pair of collectors with an adapted energy filter can increase the generated power of a hot-carrier solar cell significantly. The question arises, to which extent the addition of even further collector pairs is beneficial. We here analyze a situation where a series of N collector pairs is connected to the absorber with thin, energetically adjacent boxcar-shaped energy filters.

We focus on the lossless case with $f_{\text{abs}} = f_{\text{sun}}$. Each collector $\alpha = 1, \dots, N-1$ is connected to the absorber by an energy filter with width $2\delta\varepsilon$ centered around energy E_α . The transmissions hence read

$$D_{\text{sun},\alpha}(\varepsilon) = 1 \quad \text{for } E_\alpha - \delta\varepsilon < \varepsilon < E_\alpha + \delta\varepsilon \quad (8)$$

and zero otherwise. The N th filter is a step function at energy $E_{N-1} + \delta\varepsilon$, which hence transmits all high-energy charge carriers that are not transmitted to other filters.

We now proceed as in the main text and optimize the power output by adjusting loads and filter positions. The maximum power as well as the optimal filter positions are represented in Fig. 6 as a function of the number of filters. One clearly sees that it is advantageous to stack filters more densely at lower energies, where the electronic-state occupation is higher in the lossless case.

The following three conclusions can furthermore be drawn from this figure: first, it is possible to enhance greatly the extracted power by adding filters. The second important insight is that only the first few filters add a substantial contribution to the optimal generated power. Finally, in order to achieve the large enhancement in the multi-filter case, the placement of these filters in energy must be optimized. While this is realistic in the few-terminal case, it would pose a substantial challenge in the limit of many terminals.

We finally calculate the limit for the power production in the limit of infinitely many terminals. We therefore now take the filter width to be small with respect to the collector temperatures. This yields the approximate current into electron collector α ,

$$I_{\text{col},\alpha} \approx \delta\varepsilon (f_{\text{abs}}(E_\alpha) - f_{\text{col},\alpha}(E_\alpha)) + O(\delta\varepsilon^2). \quad (9)$$

As a next step, one needs the value of μ_α maximizing the power $P_\alpha = I_{\text{col},\alpha} \mu_\alpha$, which is found as the solution of

$$\mu_\alpha^{\max} f'_\alpha(E_\alpha - \mu_\alpha^{\max}) + f_\alpha(E_\alpha - \mu_\alpha^{\max}) = f_{\text{abs}}(E_\alpha). \quad (10)$$

Then, the sum over the powers in collector α is

$$\sum_\alpha P_\alpha^{\max} = \sum_\alpha (\mu_\alpha^{\max})^2 f'_\alpha(E_\alpha - \mu_\alpha^{\max}) \delta\varepsilon \quad (11)$$

$$P_{N \rightarrow \infty}^{\max} = \int d\varepsilon (\mu^{\max}(\varepsilon))^2 f'(\varepsilon - \mu^{\max}(\varepsilon)), \quad (12)$$

where in the second step, we wrote the integral form by taking the limit of $\delta\varepsilon \rightarrow 0$. The result for the maximum power in the limit $N \rightarrow \infty$ is shown as black dashed line in Fig. 6, which the red line, indeed, quickly approaches.

Smooth filters

The experimentally more realistic case of smooth filters can be modeled by replacing the sharp high-pass transmission function by a smooth version $D(\varepsilon) = (1 + \exp[(\varepsilon - E_0)/w])^{-1}$, where w is the smoothness coefficient. The optimized power as a function of the filter position both in a two- and four-terminal cell in the thermoelectric regime is shown in Fig. 7. The Figure is obtained using the nonequilibrium model presented above, at $\gamma_{\text{col}} = 100\gamma_{\text{sun}}$ and all other couplings set to zero. Increasing the smoothness of the filters decreases the total power output both in the two- and four-terminal cases. This decrease only becomes substantial when w is greater than the collector temperature T_{col} .

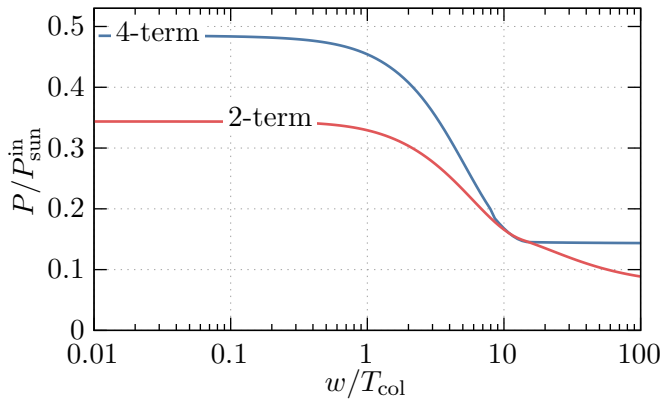


Figure 7. Power in a two and four-terminal cell, as a function of the smoothness w of the filters.

- [1] William Shockley and Hans J. Queisser, “Detailed Balance Limit of Efficiency of p-n Junction Solar Cells,” *J. Appl. Phys.* **32**, 510–519 (1961).
- [2] Peter Würfel, *Physics of Solar Cells* (Wiley-VCH, Weinheim, 2005) see Chapter 8.
- [3] Martin Green, Ewan Dunlop, Jochen Hohl-Ebinger, Masahiro Yoshita, Nikos Kopidakis, and Xiaojing Hao, “Solar cell efficiency tables (version 57),” *Prog. Photovoltaics Res. Appl.* **29**, 3–15 (2021).
- [4] Mehri Ghasemi, Joel Van Embden, Baohua Jia, and Xiaoming Wen, “Moving beyond the Shockley–Queisser limit: current bottlenecks and a new direction in solar energy conversion,” *EES Sol.* (2025), 10.1039/D5EL00053J.
- [5] Robert T. Ross and Arthur J. Nozik, “Efficiency of hot-carrier solar energy converters,” *J. Appl. Phys.* **53**, 3813–3818 (1982).
- [6] César Clavero, “Plasmon-induced hot-electron generation at nanoparticle/metal-oxide interfaces for photovoltaic and photocatalytic devices,” *Nat. Photonics* **8**, 95–103 (2014).
- [7] Dac-Trung Nguyen, Laurent Lombez, François Gibelli, Soline Boyer-Richard, Alain Le Corre, Olivier Durand, and Jean-François Guillemoles, “Quantitative experimental assessment of hot carrier-enhanced solar cells at room temperature,” *Nat. Energy* **3**, 236–242 (2018).
- [8] D. König, Y. Yao, B. Puthen-Vetttil, and S. C. Smith, “Non-equilibrium dynamics, materials and structures for hot carrier solar cells: a detailed review,” *Semicond. Sci. Technol.* **35**, 073002 (2020).
- [9] Jonatan Fast, Urs Aeberhard, Stephen P. Bremner, and Heiner Linke, “Hot-carrier optoelectronic devices based on semiconductor nanowires,” *Appl. Phys. Rev.* **8**, 021309 (2021).
- [10] Kamal Kumar Paul, Ji-Hee Kim, and Young Hee Lee, “Hot carrier photovoltaics in van der waals heterostructures,” *Nature Reviews Physics* **3**, 178–192 (2021).
- [11] Jonatan Fast, Yen-Po Liu, Yang Chen, Lars Samuelson, Adam M Burke, Heiner Linke, and Anders Mikkelsen, “Optical-beam-induced current in inas/inp nanowires for hot-carrier photovoltaics,” *ACS Applied Energy Materials* **5**, 7728–7734 (2022).
- [12] Maxime Giteau, Samy Almosni, and Jean-François Guillemoles, “Hot-carrier multi-junction solar cells: a synergistic approach,” *Applied Physics Letters* **120** (2022).
- [13] Priya Viji, Constantin Tormann, Clemens Göhler, and Martijn Kemerink, “Hot carrier organic solar cells,” *Energy & Environmental Science* **17**, 8683–8690 (2024).
- [14] While “hot-carrier” is the standard terminology, this high-energy carrier state is *rarely* a thermal distribution with a well-defined temperature.
- [15] Ludovico Tesser, Robert S. Whitney, and Janine Splettstoesser, “Thermodynamic performance of hot-carrier solar cells: A quantum transport model,” *Phys. Rev. Appl.* **19**, 044038 (2023).
- [16] Fabienne Michelini, Adeline Crépieux, and Katawoura Beltako, “Entropy production in photovoltaic-thermoelectric nanodevices from the non-equilibrium Green’s function formalism,” *J. Phys.: Condens. Matter* **29**, 175301 (2017).
- [17] Tahereh Nemati Aram, Asghar Asgari, Matthias Ernzerhof, Pascal Quémerais, and Didier Mayou, “Quantum modeling of two-level photovoltaic systems,” *EPJ Photovoltaics* **8**, 85503 (2017).
- [18] Nicolas Cavassilas, Imam Makhfudz, Anne-Marie Daré, Michel Lannoo, Guillaume Dangois, Marc Bescond, and Fabienne Michelini, “Theoretical demonstration of hot-carrier operation in an ultrathin solar cell,” *Physical Review Applied* **17**, 064001 (2022).
- [19] Zhenbang Dai and Andrew M Rappe, “Recent progress in the theory of bulk photovoltaic effect,” *Chemical Physics Reviews* **4** (2023).
- [20] Thomas Mueller and Ermin Malic, “Exciton physics and device application of two-dimensional transition metal dichalcogenide semiconductors,” *npj 2D Mater. Appl.* **2**, 1–12 (2018).
- [21] Md Roknuzzaman, Kostya Ostrikov, Hongxia Wang, Aijun Du, and Tuquabo Tesfamichael, “Towards lead-free perovskite photovoltaics and optoelectronics by ab-initio simulations,” *Scientific reports* **7**, 14025 (2017).
- [22] Vinod Kumar Solet and Sudhir K Pandey, “Many-body ab initio study of quasiparticles, optical excitations, and excitonic properties in li zn as and sc ag c for photovoltaic applications,” *Physical Review Applied* **23**, 064040 (2025).
- [23] Michael V. Moskalets, *Scattering Matrix Approach to Non-Stationary Quantum Transport* (World Scientific Publishing Company, London, England, UK, 2011).
- [24] Ya. M. Blanter and M. Büttiker, “Shot noise in mesoscopic conductors,” *Phys. Rep.* **336**, 1–166 (2000).
- [25] O. Entin-Wohlman, Y. Imry, and A. Aharony, “Three-terminal thermoelectric transport through a molecular junction,” *Phys. Rev. B* **82**, 115314 (2010).
- [26] Rafael Sánchez and Markus Büttiker, “Optimal energy quanta to current conversion,” *Phys. Rev. B* **83**, 085428 (2011).
- [27] Björn Sothmann, Rafael Sánchez, and Andrew N. Jordan, “Quantum Nernst engines,” *Europhys. Lett.* **107**, 47003 (2014).
- [28] Francesco Mazza, Riccardo Bosio, Giuliano Benenti, Vittorio Giovannetti, Rosario Fazio, and Fabio Taddei, “Thermoelectric efficiency of three-terminal quantum thermal machines,” *New J. Phys.* **16**, 085001 (2014).

- [29] Robert S. Whitney, “Quantum Coherent Three-Terminal Thermoelectrics: Maximum Efficiency at Given Power Output,” *Entropy* **18**, 208 (2016).
- [30] Giuliano Benenti, Giulio Casati, Keiji Saito, and Robert S. Whitney, “Fundamental aspects of steady-state conversion of heat to work at the nanoscale,” *Phys. Rep.* **694**, 1–124 (2017).
- [31] Rafael Sánchez, Janine Splettstoesser, and Robert S. Whitney, “Nonequilibrium System as a Demon,” *Phys. Rev. Lett.* **123**, 216801 (2019).
- [32] Fatemeh Hajiloo, Rafael Sánchez, Robert S. Whitney, and Janine Splettstoesser, “Quantifying nonequilibrium thermodynamic operations in a multiterminal mesoscopic system,” *Phys. Rev. B* **102**, 155405 (2020).
- [33] Rafael Sánchez, Peter Samuelsson, and Patrick P. Potts, “Autonomous conversion of information to work in quantum dots,” *Phys. Rev. Res.* **1**, 033066 (2019).
- [34] Sergio Ciliberto, “Autonomous out-of-equilibrium Maxwell’s demon for controlling the energy fluxes produced by thermal fluctuations,” *Phys. Rev. E* **102**, 050103 (2020).
- [35] Nahuel Freitas and Massimiliano Esposito, “Characterizing autonomous Maxwell demons,” *Phys. Rev. E* **103**, 032118 (2021).
- [36] Sebastian E. Deghi and Raúl A. Bustos-Marín, “Entropy current and efficiency of quantum machines driven by nonequilibrium incoherent reservoirs,” *Phys. Rev. B* **102**, 045415 (2020).
- [37] Multiplying by k_B^2/\hbar to get SI units, gives $P_{\text{sun}}^{\text{in}} = 8.5 \mu\text{W}$ at $\gamma_{\text{sun}} = 1$.
- [38] Ludovico Tesser, *Fluctuations and nonequilibrium thermodynamics in electronic nanosystems* (Licentiate Thesis, Chalmers University of Technology, 2022) 532253.
- [39] Robert S. Whitney, “Finding the quantum thermoelectric with maximal efficiency and minimal entropy production at given power output,” *Phys. Rev. B* **91**, 115425 (2015).
- [40] Boxcar-shapes could be implements with narrow bandgap materials [45] or nanostructures [39].
- [41] S. M. Sze and Kwok K. Ng, *Physics of Semiconductor Devices* (2006).
- [42] M. Büttiker, “Small normal-metal loop coupled to an electron reservoir,” *Phys. Rev. B* **32**, 1846–1849(R) (1985).
- [43] M. Büttiker, “Role of quantum coherence in series resistors,” *Phys. Rev. B* **33**, 3020–3026 (1986).
- [44] David Sánchez and Llorenç Serra, “Thermoelectric transport of mesoscopic conductors coupled to voltage and thermal probes,” *Phys. Rev. B* **84**, 201307 (2011).
- [45] Jun Zhou, Ronggui Yang, Gang Chen, and Mildred S Dresselhaus, “Optimal bandwidth for high efficiency thermoelectrics,” *Physical review letters* **107**, 226601 (2011).